AGU PUBLICATIONS

Water Resources Research

RESEARCH ARTICLE
10.1002/2016WR018724

Impact of kinetic mass transfer on free convection in a porous medium

Chunhui Lu[1,2], Liangsheng Shi[1], Yiming Chen[3], Yueqing Xie[4,5], and Craig T. Simmons[4,5]

[1]State Key Laboratory of Water Resources and Hydropower Engineering Science, Wuhan University, Wuhan, China, [2]State Key Laboratory of Hydrology-Water Resources and Hydraulic Engineering, Hohai University, Nanjing, China, [3]World Bank, Washington, District of Columbia, USA, [4]School of the Environment, Flinders University, Adelaide, South Australia, Australia, [5]National Centre for Groundwater Research Training, Flinders University, Adelaide, South Australia, Australia

Key Points:
- A dual-domain transfer model is first applied to an unstable variable-density flow system
- Density-driven transport and mass transfer are two controlling mechanisms of solute loading
- The effect of kinetic mass transfer depends on mass transfer parameters

Correspondence to:
C. Lu,
clu@hhu.edu.cn

Citation:
Lu, C., L. Shi, Y. Chen, Y. Xie, and C. T. Simmons (2016), Impact of kinetic mass transfer on free convection in a porous medium, *Water Resour. Res.*, *52*, 3637–3653, doi:10.1002/2016WR018724.

Received 3 FEB 2016
Accepted 17 APR 2016
Accepted article online 25 APR 2016
Published online 13 MAY 2016

Abstract We investigate kinetic mass transfer effects on unstable density-driven flow and transport processes by numerical simulations of a modified Elder problem. The first-order dual-domain mass transfer model coupled with a variable-density-flow model is employed to describe transport behavior in porous media. Results show that in comparison to the no-mass-transfer case, a higher degree of instability and more unstable system is developed in the mass transfer case due to the reduced effective porosity and correspondingly a larger Rayleigh number (assuming permeability is independent on the mobile porosity). Given a constant total porosity, the magnitude of capacity ratio (i.e., immobile porosity/mobile porosity) controls the macroscopic plume profile in the mobile domain, while the magnitude of mass transfer timescale (i.e., the reciprocal of the mass transfer rate coefficient) dominates its evolution rate. The magnitude of capacity ratio plays an important role on the mechanism driving the mass flux into the aquifer system. Specifically, for a small capacity ratio, solute loading is dominated by the density-driven transport, while with increasing capacity ratio local mass transfer dominated solute loading may occur at later times. At significantly large times, however, both mechanisms contribute comparably to solute loading. Sherwood Number could be a nonmonotonic function of mass transfer timescale due to complicated interactions of solute between source zone, mobile zone and immobile zone in the top boundary layer, resulting in accordingly a similar behavior of the total mass. The initial assessment provides important insights into unstable density-driven flow and transport in the presence of kinetic mass transfer.

1. Introduction

Theoretical and field studies have shown that density-driven flow and transport are ubiquitous in groundwater systems [e.g., *Wood and Hewett*, 1984; *Schincariol and Schwartz*, 1990; *Koch and Zhang*, 1992; *Liu and Dane*, 1996; *Yang and Edwards*, 2000; *Simmons et al*., 2001; *Holzbecher*, 2005; *Simmons*, 2005; *Stevens et al*., 2009; *Van Dam et al*., 2009]. Free convection occurs when the flow is driven purely by buoyancy forces resulting from the interactions between the density difference and gravitational field, and is therefore completely dependent on the concentration field for a solute transport problem. The presence of a dense fluid overlying a lighter one may lead to significant density gradients, onset of gravity-driven instabilities, and ultimately free downward convection of the dense fluid. In comparison to diffusion, this process takes place over larger spatial scales and shorter timescales, exhibiting an effective mechanism for solute transport and mixing. There are numerous well-documented examples of free convection processes in reality [e.g., *Frind*, 1982; *Zhang and Schwartz*, 1995; *Simmons and Narayan*, 1997; *Wooding et al*., 1997; *Kooi et al*., 2000]. In coastal hydrogeological systems, for example, a typical example of free convection is the nature setting where saltwater overlies freshwater because of tides, floods, or shoreline migration [e.g., *Stevens et al*. 2009]. It is also well studied and documented in salt lakes and saline disposal basins [e.g., *Simmons and Narayan*, 1997; *Van Dam et al*., 2009].

With the emergence of many practical problems in groundwater resources management, the studies of solute transport in porous media driven by free convection have been conducted intensively during the past decade [e.g., *Park and Aral*, 2003; *Post and Prommer*, 2007; *Xie et al*., 2010, 2011, 2012; *Ataie-Ashtiani et al*., 2014]. Among these studies, the role of spatial heterogeneity in permeability has received broad attention [e.g., *Schincariol et al*., 1997; *Schincariol*, 1998; *Simmons et al*., 2001; *Prasad and Simmons*, 2003; *Nield and*

Simmons, 2007; *Simmons et al*., 2008; *Sharp and Shi*, 2009; *Post and Simmons*; 2010]. Previous studies have examined the effect of discrete fractures and showed that fracture network characteristics such as fracture density and connectedness have a controlling influence on unstable free convection [e.g., *Shikaze et al*., 1998; *Graf and Therrien*, 2005; *Simmons et al*., 2008; *Vujevic et al*., 2014]. Research was also carried out to analyze the effects of boundary conditions [*Park and Aral*, 2003; *Xie et al*., 2010; *Ataie-Ashtiani et al*., 2014; *Liu et al*., 2015], and multicomponent geochemical reactions [*Post and Prommer*, 2007]. With no doubt, these studies provide insights into processes and mechanisms that govern solute transport driven by free convection. To the best of our knowledge, however, no studies have been undertaken to evaluate the potential impacts of kinetic mass transfer (i.e., mass exchange processes between mobile and relatively immobile zones due to low-permeability zones, dead-end pores, etc.) on unstable density-driven solute loading processes, despite that it exists prevalently in natural subsurface environments over various scales ranging from pore scale to field scale and has been shown to be a potentially limiting factor controlling the process of solute transport [e.g., *Feehley et al*., 2000; *Culkin et al*., 2008; *Lu et al*., 2009, 2011].

Transport model with mass transfer descriptions usually conceptualize a porous or fractured medium as consisting of two overlapping continuous media: a mobile domain, where advective-dispersive transport occurs, and a relatively immobile one with a continuous withdrawal and return of solute mass [*Coats and Smith*, 1964; *van Genuchten and Wierenga*, 1976]. Mass transfer between mobile and immobile domains is kinetically controlled. Such a transport model is usually termed a dual-domain mass transfer (DDMT) model, which has received increasing attention in recent years because: (1) it has proven effective at characterizing various pore-scale diffusion processes between relative mobile and immobile domains, in which the latter may consist of sorption regions, dead-end pores, porous particles, aggregates, fractures, or macropores [e.g., *Chen and Wagenet*, 1995; *Haggerty and Gorelick*, 1995; *Carrera et al*., 1998; *Haggerty et al*., 2000; *Salamon et al*., 2006], and (2) in the absence of sufficient aquifer characterization, the DDMT model may be used to describe extreme asymmetric concentration profiles in anomalous transport caused by aquifer heterogeneity, therefore offering a physically based alternative to the classical advection-dispersion model [e.g., *Berkowitz and Scher*, 1997, 1998; *Harvey and Gorelick*, 2000; *Dentz and Berkowitz*, 2003; *Zinn et al*., 2004]. Studies have shown that numerical models based on different conceptual models of solute transport (including the DDMT model, equivalent porous medium model, and discrete fracture matrix diffusion model) can all be calibrated capable of reproducing well-observed contaminant distributions (with negligible density effects) in a porous medium that contains fractures or macrospores [e.g., *Chambon et al*., 2011; *Blessent et al*., 2014].

As a simplest approximation, the first-order DDMT models are often employed by practitioners to describe kinetic mass transfer processes. Other mass transfer models are also available for describing various asymmetric transport behaviors. *Haggerty and Gorelick* [1995] proposed a multirate model by superimposing a distribution of first-order mass transfer rates to characterize incomplete mixing in the immobile domain and various diffusion processes. Based on the same belief of pore-scale heterogeneity, *Carrera et al*. [1998] developed a more versatile model of linear mass transfer, in which mass transfer are described by a convolution product of concentrations in the mobile domain and a memory function rather than predefining the mass transfer model. By choosing appropriate memory functions, the model can reproduce the first-order, multirate, sphere, layer or cylinder diffusive models [e.g., *Carrera et al*., 1998; *Haggerty et al*., 2000].

Despite substantial research, previous studies of DDMT focussed mainly on constant-density flow and transport problems and little work has been conducted to examine solute transport in variable-density flow scenarios. To the best of our knowledge, only *Lu et al*. [2009] and *Lu and Luo* [2010] considered such an effect on seawater intrusion and showed numerically that DDMT may widen significantly the thickness of a moving freshwater-seawater interface. As pointed out above, however, the role of kinetic mass transfer on unstable density-driven flow and transport is unknown. Neglecting this effect may result in an error in estimating solute loading rate as well as mixing processes in subsurface environments. Therefore, an initial assessment of such an effect on free convection processes is clearly needed.

In the present study, we first conduct a systematic investigation on the effects of DDMT on free convection processes by using the first-order DDMT model, coupled with the variable-density-flow model to describe solute transport behavior in porous media. The finite difference code SEAWAT-2000 [*Langevin et al*., 2003] is employed to conduct numerical simulations. The main objective of this study is to explore how the presence of the immobile domain and associated kinetic mass transfer affects solute loading. Specifically, we

quantify the plume behavior in mobile and immobile domains, compare simulation results between cases with and without a DDMT, and assess the importance of DDMT parameters including capacity ratio (immobile porosity/mobile porosity) and mass transfer rate coefficient in controlling solute transport in porous media.

The classic Elder problem, a widely known and commonly used example for studying free convection, is modified to implement the proposed research. Following previous studies on free convection by *Prasad and Simmons* [2003, 2005] and *Xie et al*. [2010, 2011, 2012], we quantify various measurable characteristics of simulation results, such as Sherwood Number, total mass of solute, and solute centre of gravity. Importantly, these measurable characteristics in the mobile, immobile and total domains (i.e., both mobile and immobile domains) will be quantified respectively and compared.

2. Dual-Domain Mass Transfer

DDMT models have been widely used to describe solute transport behavior in the subsurface where traditional advection-dispersion models are inadequate [e.g., *Liu et al*., 2007]. The equation for advection-dispersion transport, coupled with the first-order mass transfer is expressed as [*Coats and Smith*, 1964; *van Genuchten and Wierenga*, 1976]:

$$\theta_m \frac{\partial C_m}{\partial t} + \theta_{im} \frac{\partial C_{im}}{\partial t} = \nabla \cdot (\theta_m \mathbf{D} \cdot \nabla C_m) - \nabla \cdot (\theta_m \mathbf{v} C_m) + q_s C_s \tag{1a}$$

$$\theta_{im} \frac{\partial C_{im}}{\partial t} = \xi (C_m - C_{im}) \tag{1b}$$

where θ_m and θ_{im} are the porosities of the mobile and immobile domains, respectively; C_m [ML^{-3}] is the dissolved concentration in the mobile domain; C_{im} [ML^{-3}] is the dissolved concentration in the immobile domain; ξ [T^{-1}] is the first-order mass transfer rate coefficient; $\mathbf{D}$ [L^2T^{-1}] is the hydrodynamic dispersion coefficient tensor; $\mathbf{v}$ [LT^{-1}] is the vector of the seepage velocities; and q_s [T^{-1}] and C_s [ML^{-3}] are the flow rate per unit volume of aquifer and concentration of the source/sink, respectively. As pointed out by *Liu et al*. [2007], for more complex field conditions, a higher order diffusion equation or first-order multirate equation may be applied [*Haggerty and Gorelick*, 1995].

Equations (1a) and (1b) describe that transport of solute in the mobile domain is dominated by advection, while transport in the immobile domain is controlled by a diffusion-type equation. Porosity at any representative elementary volume is characterized by mobile porosity (θ_m) and immobile porosity (θ_{im}), with total porosity (θ_t) being $\theta_m + \theta_{im}$. The connection between fluids in the mobile and immobile domain is through a mass transfer rate coefficient ξ, which controls the speed of mass transfer between the two domains. The magnitude of this coefficient mainly depends on characteristics of the porous medium and solute species.

For cases with a very low ξ, dual-domain transport models collapse to single domain models with the effective porosity being θ_m, since the immobile zone is almost nullified. For cases with a very high ξ, by contrast, instantaneous transport between the mobile and immobile regions occurs. Therefore, transport models that incorporate dual domain also collapse to single domain models with an effective porosity being θ_m, and at the same time with a retardation factor R given by $1+\beta$, where $\beta = \theta_{im}/\theta_m$, known as the capacity ratio [*Neville*, 2006].

3. Conceptual Model and Numerical Modeling

3.1. Modified Elder Problem

The Elder problem was originally designed for heat flow [*Elder*, 1967], but later recast by *Voss and Souza* [1987] as a variable-density groundwater flow problem. The former and latter here refer to the original and classic Elder problem, respectively. The Elder problem has become one of the most popular benchmark tests for validating newly developed numerical codes simulating variable density flow and transport in porous media [e.g., *Voss and Souza*, 1987; *Park and Aral*, 2003; *Thorne and Sukop*, 2004]. Our modified Elder problem is shown in Figure 1, which shares the same definition of the domain geometry and boundary conditions as those in the work of *Post and Prommer* [2007]. As shown, a vertical section of freshwater-saturated porous media extends 600 m in the horizontal direction and 150m in the vertical direction. The

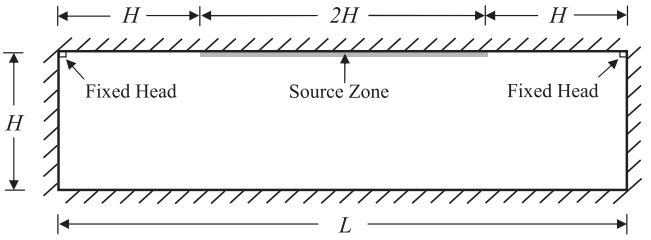

Figure 1. Model geometry and boundary conditions for the modified Elder problem. All boundaries are impermeable. The source zone is located at the middle half of the top boundary. There is one fixed head node at the top left and right corner, respectively.

source zone is located at the middle half of the top boundary, which can cause onset of the instability and mass flux into the aquifer system by molecular diffusion. As a general assumption, the density of the source (ρ_{source}) is 1200 kgm^{-3}, which corresponds to a salinity of 280 kgm^{-3} by applying a linear function of state:

$$\rho = \rho_0 + \varepsilon C_m \quad (2)$$

where ε is dimensionless constant with a value of 0.7143 for salt concentration [*Langevin et al.*, 2003]; and ρ_0 [ML^{-3}] and ρ [ML^{-3}] are reference freshwater and actual fluid densities, respectively. Note that the value of the concentration adopted is considerably high, in comparison to a common seawater concentration (usually around 35 kgm^{-3}). This value is selected here as it is used in the classic Elder problem, and has been employed in many later studies [e.g., *Post and Prommer*, 2007; *Xie et al.*, 2011]. With the increase of solute mass in the system, the flow is then driven by density gradients in the mobile domain.

The boundary condition at the bottom of the model domain is different from that in the classic Elder problem and altered to a no-flux boundary (i.e., an impermeable boundary) because this scenario more approaches the realistic condition [*Post and Prommer*, 2007]. Two outlet cells with fixed head are specified at the top left and right corners, allowing an outlet for fluid and salt mass. A homogeneous, isotropic aquifer is assumed to comprise two interacting domains: mobile and immobile domains. Accordingly, the total porosity is divided into two parts: mobile and immobile porosities. As noted above, the link between the mobile and immobile zones is through a mass transfer rate coefficient (ξ). A broad range of values of capacity ratios ($\beta = 0$, 0.25, 1, and 4) and mass transfer rate coefficients ($\xi = 1.0 \times 10^{-3} \sim 1.0 \times 10^{-6}$ d^{-1}) were selected to conduct sensitivity analysis, together with other simulation parameters listed in Table 1. When varying β, the value of $\theta_t = 0.1$ is kept constant. It should be noted that the values of capacity ratio and the orders of magnitude of mass transfer parameters assumed are comparable to those calibrated values in different field tests [e.g., *Feehley et al.*, 2000; *Culkin et al.*, 2008; *Liu et al.*, 2007; *Gong et al.*, 2010]. To focus on the impact of kinetic mass transfer, we first assume that permeability is independent on the mobile porosity. Then, a simple relationship between permeability and the mobile porosity is considered to demonstrate the coupled effect of changing the mobile porosity and permeability on solute loading.

Table 1. Simulation Parameters Used in Modified Elder Problem[a]

Parameter	Variable	Value	Unit
Model length	L	600	M
Model height	H	150	M
Intrinsic permeability	k	4.845×10^{-13}	m^2
Total porosity	θ_t	0.1	
Mobile porosity	θ_m	0.02, 0.05, 0.08, 0.1[a]	
Immobile porosity	θ_{im}	$\theta_t - \theta_m$	
Capacity ratio	$\beta = \theta_{im}/\theta_m$	0[a], 0.25, 1, 4	
Mass transfer rate coefficient	ξ	$1.0 \times 10^{-3} \sim 1.0 \times 10^{-6}$	d^{-1}
Longitudinal dispersivity	α_L	0	M
Transverse dispersivity	α_T	0	M
Molecular diffusion coefficient	D_d	3.565×10^{-6}	m^2 s^{-1}
Dynamic viscosity	μ	1.0×10^{-3}	kg m^{-1} s^{-1}
Gravitational acceleration	g	9.81	m s^{-2}
Specific storage	S_s	1.0×10^{-4}	m^{-1}
Freshwater density	ρ_0	1000	kg m^{-3}
Source density at the top boundary	ρ_{source}	1200	kg m^{-3}
Source concentration at the top boundary	C_{source}	280	kg m^{-3}

[a]No-mass-transfer case.

3.2. Instability Descriptor

The stratification of a dense fluid overlying a lighter fluid can give rise to the onset of gravity-driven instabilities. A commonly used descriptor of instability for the Elder problem is the dimensionless Rayleigh number (*Ra*) given by [e.g., *Simmons et al*., 2001]:

$$Ra = \frac{k\rho_0 g\alpha H}{\mu\theta D_d} \tag{3}$$

where k [L^2] is intrinsic permeability; g [LT^{-2}] is acceleration due to gravity; $\alpha=(\rho_{source}-\rho_0)/\rho_0$ is the density contrast coefficient; H [L] is the vertical extent of the flow regime; μ [$ML^{-1}T^{-1}$] is dynamic viscosity; D_d [L^2T^{-1}] is the aqueous molecular diffusion coefficient; and θ is effective porosity, and equal to θ_m in the dual-domain model. The critical *Ra* is 40 in the Horton-Rogers-Lapwood problem with the infinitely extended horizontal porous layer and constant temperature at upper and lower boundaries [*Horton and Rogers*, 1945; *Lapwood*, 1948], but is zero for the classic Elder problem [*van Reeuwijk et al*., 2009; *Xie et al*., 2010]. The values of *Ra* in the classic Elder problems are around 400, which is considerably larger than the critical *Ra* and hence can cause significant free convection processes. Inclusion of the immobile zone would yield a smaller effective porosity and therefore a larger value of *Ra*, given a constant θ_t. *Xie et al*. [2011] indicated that a smaller effective porosity results in a larger plume migrate rate. The presence of the immobile domain, however, would reduce the solute mass in the mobile domain due to kinetic mass transfer and hence reduce the density-driven flow velocity. These two controlling mechanisms complicate the plume migration processes.

3.3. Modeling Tool

Several computer codes are available for simulating variable density flow and solute transport. SEAWAT-2000 is chosen here because it is developed by combining MODFLOW-2000 and MT3DMS into a single computer program and the latter is a program implemented with an optional, dual-domain formulation for modelling mass transport [*Langevin et al*., 2003]. The DDMT model coupled with the variable-density-flow model has been previously used in studying the movement of the freshwater-seawater mixing zone [*Lu et al*., 2009; *Lu and Luo*, 2010].

3.4. Spatial and Temporal Discretization

Previous studies on the Elder problem have pointed out that the grid size is a critical factor controlling the accuracy of simulated plume profile [e.g., *Voss and Souza*, 1987; *Park and Aral*, 2003; *Prasad and Simmons*, 2005]. More recently, *van Reeuwijk et al*. [2009] showed that multiple bifurcation states are possible and suggested numerical controls such as discretization may be important in selecting states. This implies that the notion of grid convergence, aiming for a single solution is not dependent on grid size, does not make sense in the context of highly unstable fee convection problems. In the current study, a uniform grid spacing with $\Delta x=\Delta z=1m$ was used, similar to that adopted in previous studies [e.g., *Voss and Souza*, 1987; *Prasad and Simmons*, 2003; *Post and Prommer*, 2007; *Xie et al*., 2010]. Due to symmetry, numerical simulations were carried out in half of the domain in order to reduce the computational time.

Importantly, in the present study, because of the modified boundary condition at the bottom layer, the system cannot reach a steady state condition, until the whole domain is filled with pure saltwater. Therefore, the total simulation time in our study is increased to 50 years (i.e., 18,250 days), which is significantly longer than that in the classic Elder problem. For the transport steps, during which heads are considered constant, a uniform step size of 2 days is specified in the model input.

3.5. Measurable Characteristics

Several measurable characteristics, including Sherwood Number (*Sh*), total mass of solute (*TM*), solute centre of gravity (*COG*), etc. were used to quantify the simulation results in previous studies on the Elder problem [*Prasad and Simmons*, 2003, 2005; *Post and Prommer*, 2007; *Xie et al*., 2010], and will be used as well in the current study. Since there are three conceptual domains involved in the DDMT model (i.e., mobile, immobile, and total domains), each characteristic adopted is defined for these three domains. In addition, two new dimensionless parameters (nonequilibrium state index and the difference of the Sherwood Number between the mobile and immobile domains) are defined exclusively for the problems involving kinetic mass transfer, as shown below.

3.5.1. Sherwood Number (*Sh*)

Dimensionless Sherwood Number (*Sh*) is commonly employed to assess the ratio of actual mass transfer due to free convection during the transient state to the rate of mass transfer due to diffusion, and is expressed by [*Nield and Bejan*, 2006, equation (9.34)]:

$$Sh = \frac{mH}{WL_s D_d \Delta C} \tag{4}$$

where m [MT^{-1}] is the mass flux across the source boundary; W [L] is the width of the source zone and is equal to unit for the current 2D problem; L_s [L] is the length scale of the source zone; and ΔC [ML^{-3}] is the maximum concentration difference between freshwater and saltwater.

The solute diffused from the source zone into the aquifer system leads to the increase of total mass in both mobile and immobile domains. Mass flux into the mobile domain is driven mainly by density-driven transport, while mass flux into the immobile domain is completely through kinetic mass transfer from the mobile domain. Hence, the mass fluxes into the two domains may be different, depending on ξ and β. Here we define the dimensionless *Sh* for mobile and immobile domains, respectively:

$$Sh^m = \frac{m^m H}{WL_s D_d \Delta C} \tag{5}$$

$$Sh^{im} = \frac{m^{im} H}{WL_s D_d \Delta C} \tag{6}$$

where m^m [MT^{-1}] and m^{im} [MT^{-1}] are the mass flux in the mobile and immobile domains, respectively, and $m = m^m + m^{im}$, and $Sh = Sh^m + Sh^{im}$. Note that Sh^m and Sh^{im} defined do not represent diffusive fluxes, but quantify net mass fluxes in the two domains. The comparison of mass fluxes into the two domains allows one identifies the dominant mechanism for solute transport in the aquifer system. A dimensionless parameter E is defined hereby to evaluate which mechanism dominates the transient solute loading. The expression of E is given as:

$$E = Sh^m - Sh^{im} \tag{7}$$

E compares the mass fluxes in mobile and immobile domains. When $E > 0$ (i.e., the mass flux in the mobile domain is larger than in the immobile domain), mobile domain (or density-driven) dominated transport process occurs. When $E < 0$, by contrast, the mass flux in the immobile domain is larger than that in the mobile domain, indicating that solute loading is controlled by the immobile domain (or local mass transfer). Particularly, as E approaches 0, both domains contribute comparably to solute loading.

3.5.2. Total Mass of Solute (*TM*)

The total mass of solute (*TM*) is a parameter used to quantify the transient total amount of solute contained in the aquifer system. Here we define a normalized *TM*, which is similar to the definition in *Post and Prommer* [2007]:

$$TM^m = \frac{\theta_m}{(\theta_m + \theta_{im})LH} \int_{x=0}^{x=L} \int_{z=0}^{z=H} C_{x,z}^m dxdz \tag{8}$$

$$TM^{im} = \frac{\theta_{im}}{(\theta_m + \theta_{im})LH} \int_{x=0}^{x=L} \int_{z=0}^{z=H} C_{x,z}^{im} dxdz \tag{9}$$

$$TM = TM^m + TM^{im} \tag{10}$$

in which TM^m, TM^{im}, and TM are normalized total mass of solute in mobile, immobile, and total domains, respectively; and $C_{x,z}^m$ and $C_{x,z}^{im}$ are normalized concentration values in the cell (x, z) of mobile and immobile domains, respectively. Values of TM^m, TM^{im}, and TM vary between 0 and $\theta_m/(\theta_m+\theta_{im})$, 0 and $\theta_{im}/(\theta_m+\theta_{im})$, and 0 and 1, respectively. $TM^m = TM^{im} = TM = 0$ corresponds to the initial condition, that is, the entire aquifer is filled with pure freshwater in both mobile and immobile domains. $TM^m = \theta_m/(\theta_m+\theta_{im})$, $TM^{im} = \theta_{im}/(\theta_m+\theta_{im})$, and $TM = 1$ represent the case where saltwater is completely occupied in the mobile, immobile, and total domains, respectively. $\theta_m/(\theta_m+\theta_{im})$ and $\theta_{im}/(\theta_m+\theta_{im})$ represent the mobile domain and immobile domain content, respectively.

3.5.3. Nonequilibrium State Index (*NESI*)

In the presence of DDMT, unsynchronized transport behavior may occur in mobile and immobile domains, characterized by the difference of the concentration distribution between the two domains. Based on the definition of *TM*, a dimensionless nonequilibrium state index (*NESI*) is defined to evaluate the transient degree of the nonequilibrium state, which is expressed as:

$$NESI=\frac{1}{LH}\int_{x=0}^{x=L}\int_{z=0}^{z=H}\left(C_{x,z}^{m}-C_{x,z}^{im}\right)dxdz=(\theta_m+\theta_{im})\left(TM^{m}/\theta_m-TM^{im}/\theta_{im}\right)\times 100\% \tag{11}$$

By definition, *NESI* varies between 0 and 1, representing an average concentration difference between mobile and immobile domains. A higher value of *NESI* reflects a stronger nonequilibrium condition, while a lower one means the system is near the equilibrium condition. Particularly, as $NESI=0$, the system can be regarded as a perfect equilibrium condition, indicating the average concentration distribution in mobile and immobile domains are exactly the same. Conversely, $NESI=1$ represents an ideal condition that the saltwater covers the entire mobile domain, but no saltwater enters into the immobile domain.

3.5.4. Solute Centre of Gravity (*COG*)

The solute centre of gravity (*COG*) is a statistical property of a contaminant plume thatcan be calculated by the spatial moment equation. The spatial moment $M(m, n)$ of order (m, n) is given as:

$$M(m,\ n)=\sum_{j}\sum_{i}x_i^m z_j^n C_{i,j} \tag{12}$$

where the summation is performed for all rows and columns in the domain; $C_{i,j}$ is normalized concentration value of the cell (x_i, z_j); x_i [L] and z_j [L] are coordinates; and m and n are integer power exponents that define the moment order. The centre of gravity (x_0, z_0) is then calculated by:

$$x_0=M(1,\ 0)/M(0,\ 0)\ \text{and}\ z_0=M(0,\ 1)/M(0,\ 0) \tag{13}$$

Equations (12) and (13) are directly employed to define *COG* in the mobile, immobile and total domains by replacing $C_{i,j}$ with $C_{i,j}^{m}$, $C_{i,j}^{im}$, and $\left(\frac{\theta_m C_{i,j}^{m}+\theta_{im}C_{i,j}^{im}}{\theta_m+\theta_{im}}\right)$, respectively, where $C_{i,j}^{m}$ and $C_{i,j}^{im}$ are normalized mobile and immobile concentration values of the cell (x_i, z_j). Note that $x_0=300$ m for all cases due to symmetry of the model domain.

4. Results and Discussion

4.1. Effects on Plume Development

The simulation results show that the overall effects of DDMT on the transient plume profile varies significantly depending on the selected values of mass transfer parameters. As an example, Figure 2 compares the concentration distributions between the cases with and without DDMT effects where the total porosity in the DDMT cases and effective porosity in no-mass-transfer cases are assumed the same, and also compares the concentration distributions between the mobile and immobile domains for the DDMT case. As shown, the temporal plumes developed in the case incorporating kinetic mass transfer differ substantially from those in the case without such an effect. For example, the simulation results of the DDMT case indicate that after 5 years, five separate fingers below the top boundary are developed in both mobile and immobile domains, whereas only four fingers are generated in the corresponding no-mass-transfer case. Similarly, after 10 years, three separate fingers are formed for the DDMT case, while only two fingers are present in the no-mass-transfer case. A larger number of fingers in the mass transfer case represent a more unstable system, which are mainly caused by a larger *Ra* resulting from a smaller effective porosity (i.e., mobile porosity). *Flach* [2011] revealed that a larger permeability variance will lead to a lower mobile porosity by calibrating a DDMT model to a heterogeneous medium model. In this sense, our observations agree with the finding by *Prasad and Simmons* [2003], who have shown that an increase in the permeability variance can result in a greater degree of instability at earlier times. Interestingly, the snapshot after 20 years shows that the finger number in the mobile domain is increased, while only one finger exists in the no-mass-transfer case, showing an enhanced instability in the mass transfer case.

It also can be observed that the finger speed in the mobile domain is greater than that in the corresponding no-mass-transfer case at early times. This is also caused by a smaller effective porosity and hence a larger

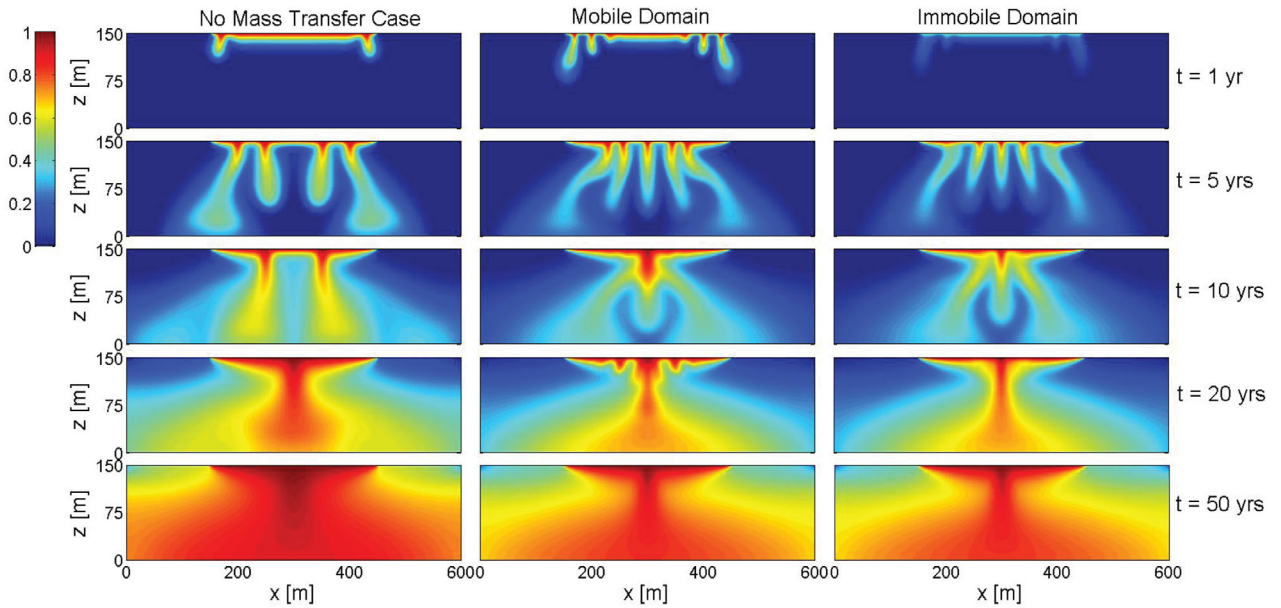

Figure 2. Concentration distributions of the cases with and without DDMT at simulation times of 1, 5, 10, 20, and 50 years. For the case including mass transfer, transient concentration distributions are shown in both mobile and immobile domains. Values of mass transfer parameters used are: β=1 and ξ=10^{-4}d^{-1}.

flow velocity. However, the presence of the immobile domain can decrease the concentration gradient at the tip of the finger and slow down the descent of solute at the later times. As a result, after 10 years most of salts are accumulated at the top of the aquifer in the DDMT cases, while substantial salts have reached the bottom of the aquifer in the case without mass transfer.

In addition, the simulation results indicate that at early times concentration distributions in the mobile and immobile domains are significantly different. Specifically, after 1 year there is negligible mass existing in the immobile domain, while substantial mass has already entered from the top source zone into the mobile domain. During this initial period free convection processes have little been affected by mass transfer processes. As time increases, the concentration contrast between the two domains becomes less and less, because the finger speed is reduced after the plume reaches aquifer bottom and the timescale of density-driven solute transport is longer than a characteristic mass transfer timescale (i.e., 1/ξ) .

Figure 3 illustrates the impacts of β and ξ on the concentration distribution in the mobile domain. The left panel demonstrates the effect of β on the plume profile. As pointed out above, a higher β corresponding to a lower effective porosity will lead to a higher *Ra*, which can cause a higher degree of instability. As expected, more fingers in the mobile domain are developed for the case with a higher β after 1.5 years. On the other hand, the cases with the same β but with different ξ have the similar evolution in the plume profile, while the magnitude of ξ only controls the evolution rate of the plume profile. For example, for the case with β=1 and ξ=10^{-4}d^{-1} and the case with β=1 and ξ=10^{-5}d^{-1}, similar plume profiles are obtained after 1.5 years (see Figures 3e and 3f). However, the fingers in the case with a lower ξ descend faster, showing weaker retention by the immobile zone. Therefore, the significant difference in the magnitude of ξ could lead to the significant difference in the transient plume profile. For example, the plume profile after 1.5 years in the case with ξ=10^{-3} d^{-1} (Figure 3b) is significantly different from that developed in the case with ξ=10^{-4} d^{-1} (Figure 3e). After 2.2 years, however, a similar plume profile is generated in the former case (Figure 3d). Obviously, there is a time lag in plume profile between the cases with the same β but with different ξ.

In addition to the assumption that θ_t is constant, one may be interested in how the value of θ_{im} affects the solute loading process in mass transfer cases with the same θ_m. To show this, three cases with θ_m=0.05 and θ_{im}=0.02, 0.05, and 0.08 are simulated with ξ=10^{-4}d^{-1} assumed. Concentration distributions in the mobile domain at simulation times of 1, 5, 10, and 20 years are shown in Figure 4. It is not surprising that the initial finger numbers are the same in three cases, because of the same *Ra*. In addition, it is obvious that a larger

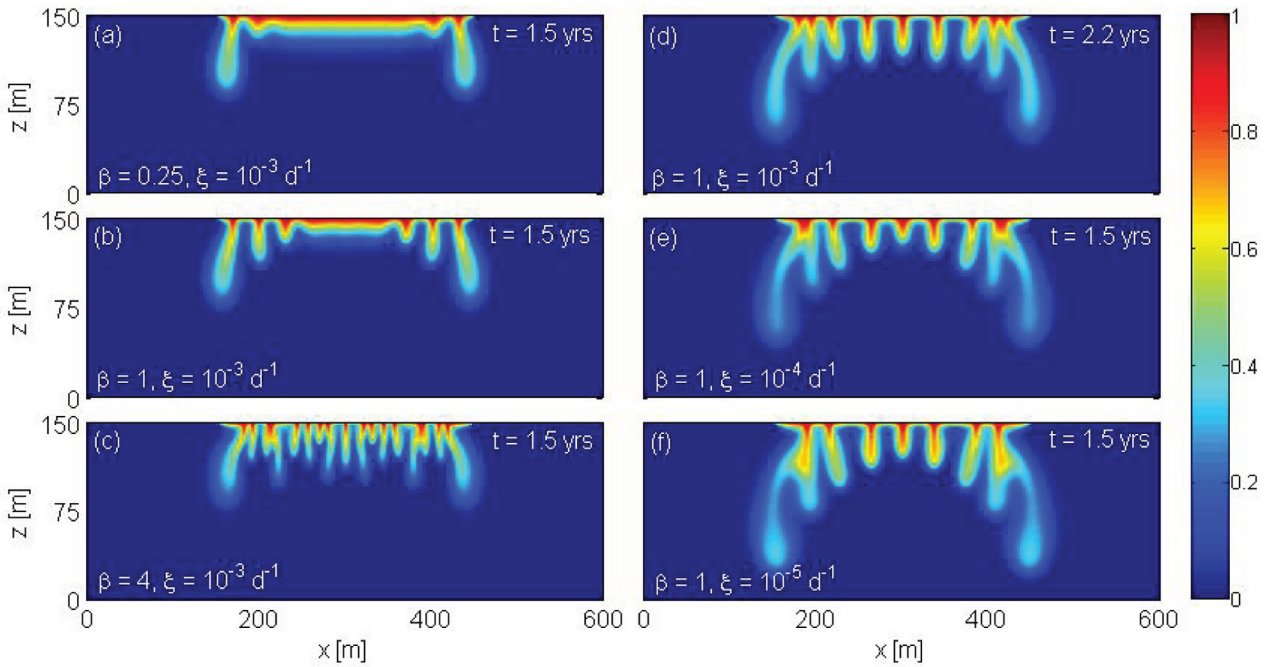

Figure 3. Concentration distributions in the mobile zone for the mass transfer cases. (a): β=0.25 and ξ=10^{-3} d^{-1}; (b) and (d): β=1 and ξ=10^{-3} d^{-1}; (c): β=4 and ξ=10^{-3} d^{-1}; (e): β=1 and ξ=10^{-4} d^{-1}; and (f): β=1 and ξ=10^{-5} d^{-1}. Simulation time is 2.2 years in Figure 3d and 1.5 years in Figures 3a, 3b, 3c, 3e, and 3f.

θ_{im} inhibits solute transport in the mobile domain. A larger θ_{im} indicates that the media contain a larger immobile volume capable of receiving mass transfer from the mobile domain, resulting in the time to reach the equilibrium condition between the mobile and immobile domains becoming longer. Therefore, the impact of a larger θ_{im} on the solute transport in the mobile domain is similar to that of a lower ξ, as also demonstrated in equation (1b). However, despite the fact that a larger θ_{im} slows down the solute transport in the mobile domain, it could lead to a higher *TM* at a later time because of a larger θ_t.

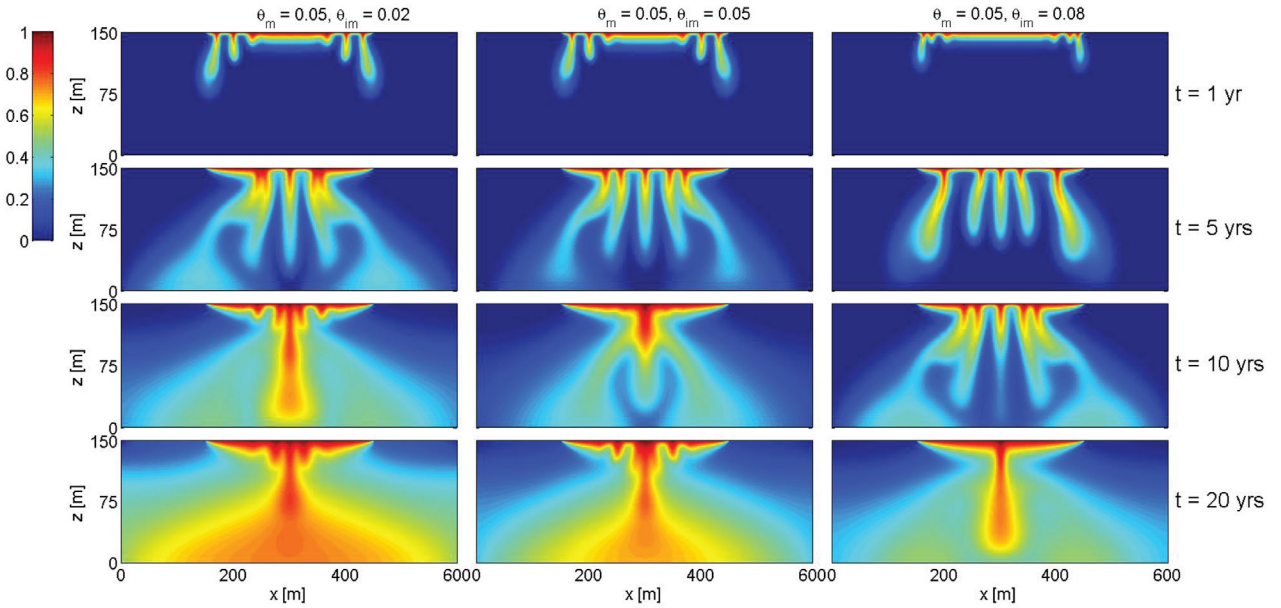

Figure 4. Concentration distributions of the mass transfer cases (ξ=$10^{-4}$$d^{-1}$) with the same mobile porosity (θ_m=0.05) but different immobile porosities (θ_{im}= 0.02, 0.05, and 0.08) at simulation times of 1, 5, 10, and 20 years.

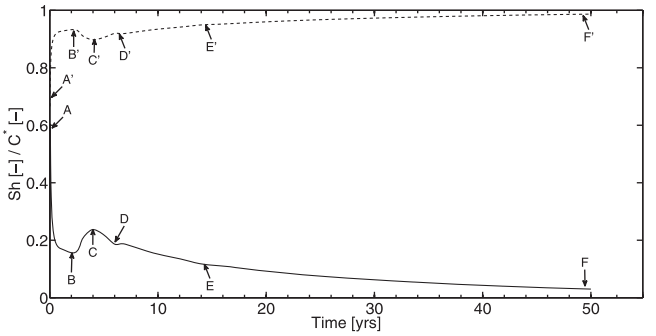

Figure 5. Sherwood Number (solid line) and the average normalized concentration in the top layer beneath the source zone (dashed line) versus time curve for the no-mass-transfer case. Points A, B, C, D, E, and F, and A′, B′, C′, D′, E′, and F′ separate five main stages.

4.2. Quantitative Assessment

4.2.1. Effects on Sherwood Number (*Sh*)

In the conceptual model, source solute enters into the aquifer system purely by molecular diffusion. Therefore, the concentration of the boundary layer beneath the source zone affects mass loading rate, i.e., the value of *Sh*. Figure 5 shows the variations of *Sh* and the average normalized concentration in the top layer (only the part beneath the source zone) versus time for the case without mass transfer. Obviously, the variation of *Sh* is inversely proportional to that of the average concentration in the top boundary layer, i.e., *Sh* decreases/increases with the increase/decrease of the average concentration in the top boundary layer.

Five main stages of solute transport processes are identified from Figure 5. At early times of the loading (A-B or A′-B′), vertical concentration gradients between the source zone and the top boundary layer are very high so that the diffusion process is fast and accordingly, the average concentration in the top boundary layer increases quickly. During this stage, the vertical concentration gradient between the source zone and adjacent zone is becoming less and less, resulting in a decreasing behavior of *Sh*. This reduction in *Sh* lasts about 2 years. By this time, the average concentration in the top boundary layer has reached over 90% of that in the source zone. As the top boundary layer accumulates more and more solutes and becomes thicker and thicker, instability fingers occur and descend into the deeper aquifer. As expected, the average concentration in the top boundary layer experiences a decline period, leading to the rebound of *Sh* (B-C or B′-C′). This stage continues about 2 years. This increasing phenomenon of *Sh* is terminated when the plume first touches the bottom. Subsequently, the average concentration in the top boundary layer increases again, followed by a sharp decrease of *Sh*. At the point D or D′, the tip of the finger reaches the bottom in the interior. As a consequence, the increasing rate of average concentration in the top boundary layer and the decreasing rate of *Sh* become mild. At the point E or E′, one thick finger is developed at the middle of the domain. From then on, the average concentration in the top boundary layer slowly increases and *Sh* slowly decreases correspondingly, forming the last stage of instability.

Figure 6 shows the sensitivity of β and ξ on Sh^t. For comparison, the evolution of *Sh* in the case without mass transfer is also provided. In general, kinetic mass transfer between the mobile and immobile domain enhances the oscillations of Sh^t curves. This oscillation behavior is more significant for the case with a higher β (see Figure 6c). For a lower β=0.25, the evolution of Sh^t is similar to that in the case without mass

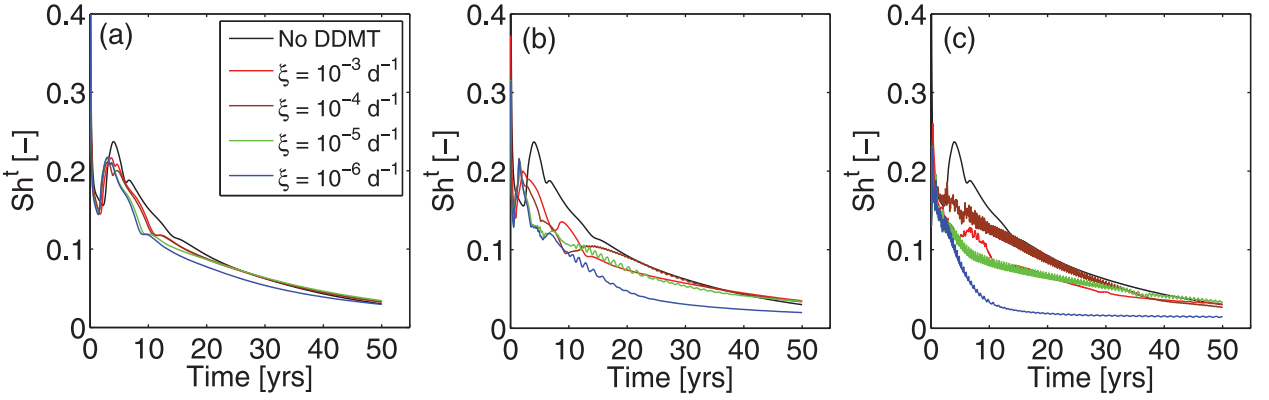

Figure 6. Sensitivity of β and ξ on Sh^t for the cases including kinetic mass transfer. The black line is the evolution of *Sh* in the case without kinetic mass transfer. (a) β=0.25; (b) β=1; and (c) β=4.

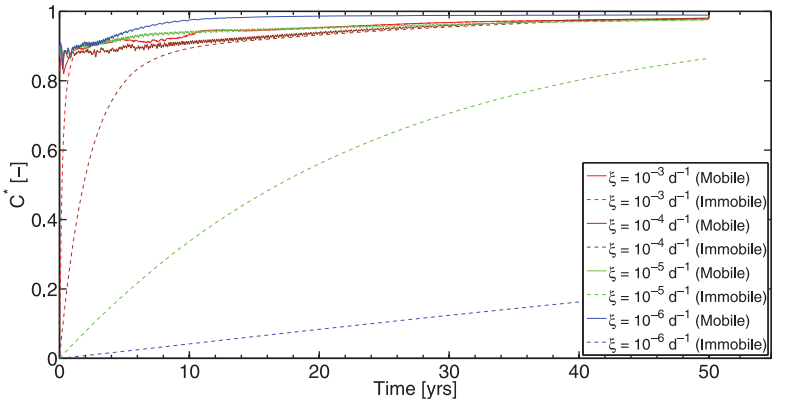

Figure 7. The average normalized concentrations in the top layer beneath the source zone versus time curve for the mass transfer case with β=4.

transfer. In addition, given a constant β the effect of ξ on Sh^t is not monotonic due to the complicated interactions between the source zone, mobile zone and immobile zone in the top boundary layer. As can be seen from Figure 6c, Sh^t of the case with ξ=10^{-4}d^{-1} is larger than that of the other mass transfer cases within a relatively long period. The reason for this phenomenon can be explained by the variation of the average concentration in the top boundary layer, which is an indicator of the variation of Sh^t.

The average normalized concentrations in the top layer beneath the source zone versus time for the mass transfer cases with β=4 are shown in Figure 7. For the critical case with ξ=10^{-4}d^{-1}, an effective mass transfer period (approximately 10 years for the current setting) is identified for the effective contribution to solute loading. This effective mass transfer process leads to the concentration in the mobile zone keeps lower than in other cases, and hence, the highest value of Sh^t in Figure 6c. For the case with ξ=10^{-3}d^{-1}, the average immobile concentration in the top boundary layer is shortly increased to nearly the same value as the corresponding mobile concentration because of the short mass transfer timescale. During this period, the average concentration in the corresponding mobile zone is decreased due to local mass transfer and then rebounded shortly to a high value due to diffusion from the source zone. From then on, solute transport in the top boundary layer is mainly driven by the density-dependent flow. For the case with an extremely large mass transfer timescale, for example ξ=10^{-6}d^{-1}, kinetic mass transfer contributes little to reducing the average concentration in the top boundary layer, leading to an average concentration in the top boundary layer that is maintained at a relatively high value and the concentration gradient between source zone and the top boundary layer is very low. Consequently, Sh^t is the lowest in Figure 6c. Note that previous studies on DDMT have also shown a nonmonotonic effect of ξ on the transport behavior [*Culkin et al.*, 2008; *Lu et al.*, 2009, 2011].

4.2.2. Mechanism Controlling Solute Transport

Figure 8 shows the sensitivity of β and ξ on E. As shown, both parameters have a significant impact on E than on ξ. For a small β, for example β=0.25, E is positive within the simulation period for all four mass

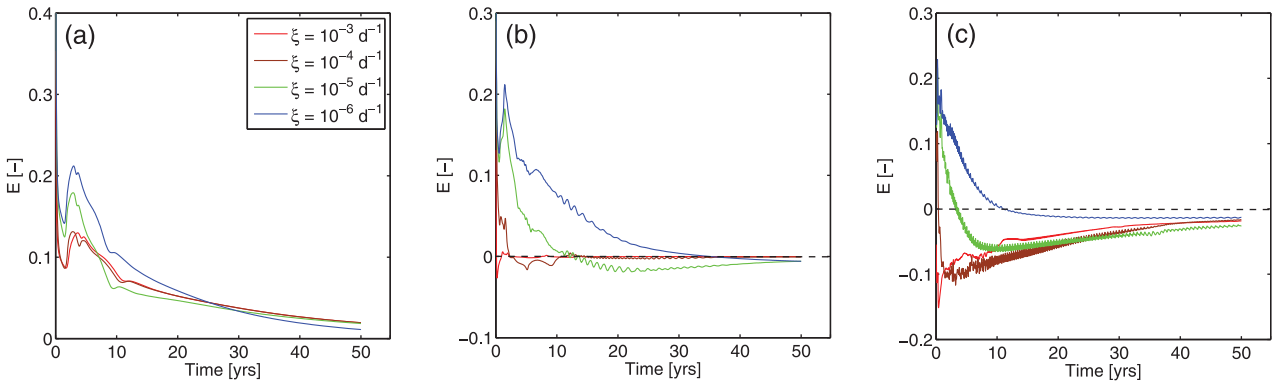

Figure 8. Sensitivity of β and ξ on E. (a) β=0.25; (b) β=1; and (c) β=4.

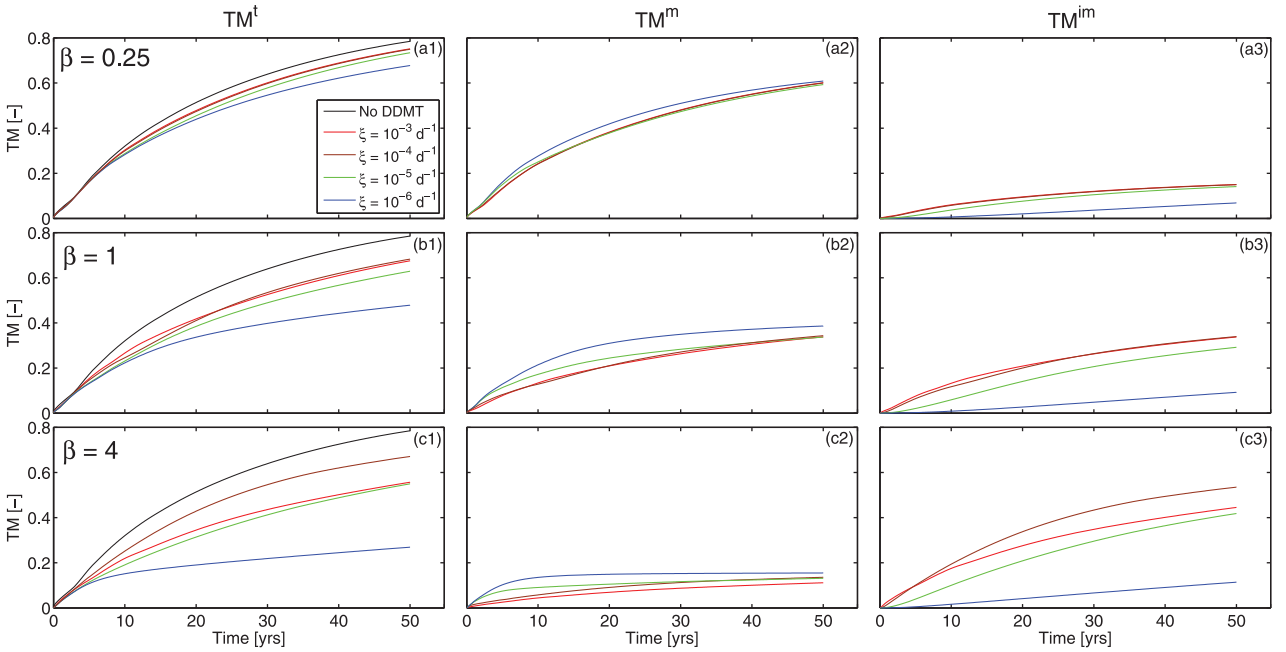

Figure 9. Sensitivity of β and ξ on the *TM*. The black line is the evolution of the *TM* in the case without kinetic mass transfer. (a) β=0.25; (b) β=1; and (c) β=4.

transfer cases, indicating that the mass flux into the mobile domain is significantly greater than into the immobile domain, and hence, density-driven transport controls the solute loading. However, with the increase of β, negative *E* occurs, which means that kinetic mass transfer from the mobile domain into the immobile domain contributes greater solute loading than density-driven transport. At large loading times, *E* for all cases approaches zero, implying that both mechanisms control comparably the solute loading. On the other hand, it is not surprising that a smaller ξ results in a higher value of *E* for all cases, because it would lead to weaker mass transfer into the immobile domain.

4.2.3. Effects on Total Mass (*TM*)

Figure 9 shows the sensitivity of β and ξ on the *TM* in total, mobile and immobile domains. In comparison to the *TM* of the no-mass-transfer case, as shown, the inclusion of the immobile zone and associated kinetic mass transfer decreases the transient *TM* in the aquifer system. For a small β=0.25 (Figure 9a1), the difference in the *TM* between the mass transfer case and no-mass-transfer case is small and also the effect of the magnitude of ξ on the *TM* is small, particularly at early loading times. However, the variability of the *TM* in the total domain is enhanced with increasing β. It is obvious that this variability is mainly caused by the variability of the *TM* in the immobile domain. Furthermore, the *TM* evolution could be a nonmonotonic function of ξ. In Figure 9c1, for example, the *TM* in the total and immobile domains of the case with ξ=10^{-4}d^{-1} maintains the largest among the mass transfer cases. This nonmonotonic behavior of ξ on the *TM* is similar to the effect on *Sh*. It is also that the *TM* curves could be overlap (Figure 9b1), showing a complex system behavior due the presence of the immobile domain.

4.2.4. Effects on Nonequilibrium State Index (*NESI*)

Figure 10 shows the sensitivity of β and ξ on the *NESI*. Initially, *NESI*=0 for all cases, representing that there is no solute in the aquifer system at the initial condition. As solute enters into the mobile domain, the average concentration contrast between mobile and immobile domains characterized quantitatively by the value of the *NESI* continuously increases until reaching a maximum. This increasing duration is shorter for the case with a larger ξ. After that, the value of the *NESI* tends to decrease, although there are some oscillations existing in the cases with a high ξ. ξ dominates the value of the *NESI*; β also affects the value of the *NESI*, to a lesser extent. Specifically, a smaller ξ and a higher β will lead to a greater *NESI*. A smaller ξ inhibits mass transfer into the immobile domain and a higher β facilitates solute transport in the mobile domain due to a smaller effective porosity. As a result, the difference of the concentration distribution between the two domains is more significant, and therefore, a larger *NESI*. At sufficiently large times, the *NESI* for all cases approaches zero because both mobile and immobile domains will be eventually filled by saltwater.

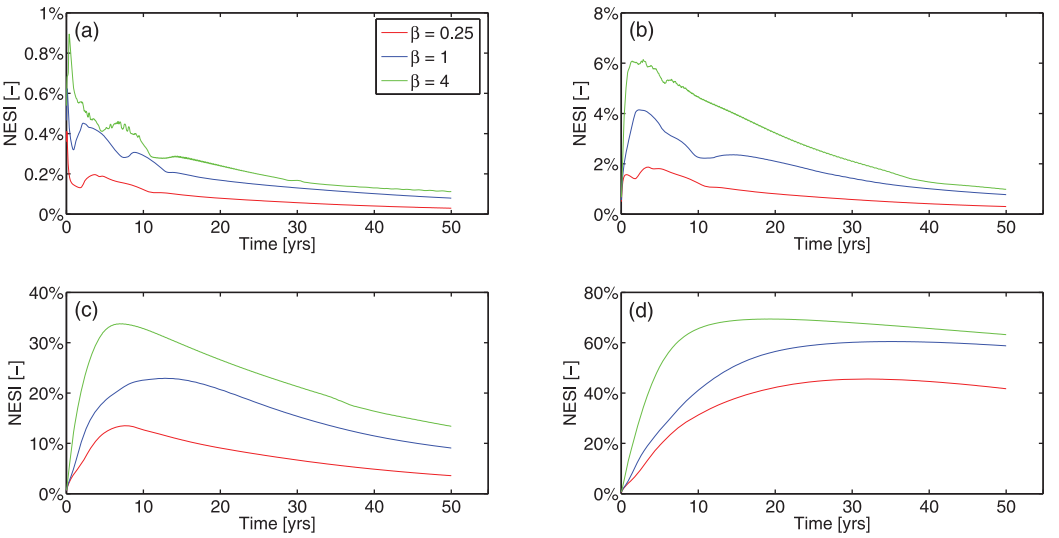

Figure 10. Sensitivity of β and ξ on the *NESI*. (a) $\xi=10^{-3}d^{-1}$; (b) $\xi=10^{-4}d^{-1}$; (c) $\xi=10^{-5}d^{-1}$; and (d) $\xi=10^{-6}d^{-1}$.

4.2.5. Effects on Solute Centre of Gravity (*COG*)

Figure 11 shows the sensitivity of β and ξ on temporal trends in *COG*. In all cases, the *COG* initially decreases because of the descent of the first salt fingers and then slightly rebounds after the first fingers touch the bottom of the aquifer. The timescale for the *COG* to achieve the minimum varies depending on the magnitudes of β and ξ. In general, this timescale is shorter for the case with a larger β and a smaller ξ, because the former results in a smaller mobile porosity and the later inhibits mass transfer, which facilitates the density-driven transport in the mobile domain. It is shown that the minimum *COG* in the case with $\beta=4$ and $\xi=10^{-3}d^{-1}$ is significantly lower than in other mass transfer cases (Figure 11a1). Similar to the case without mass transfer effects, the *COG* in all mass transfer cases asymptotically approaches the vertical centre (75 m) of the domain with increasing time of the solute loading.

Comparing the *COG* in different domains, it is found that the *COG* in the total domain has a similar trend to that in the mobile domain, which indicates that the solute plume in the mobile domain controls the *COG* in the total domain. To some extent, the difference in *COG* between the mobile and immobile domains reflects the equilibrium state of the system. Similar to *NESI*, the difference in *COG* between the two domains is dominated by ξ and is more significant in the case with a smaller ξ, while it becomes less with increasing simulation time. In the cases with a high ξ, however, the *COG* curves in the mobile, immobile and total domains almost coincide (see Figures 10a1, 10b1, and 10c1), implying that the solute plumes in the mobile and immobile domains descend simultaneously because of the fast mass transfer rate.

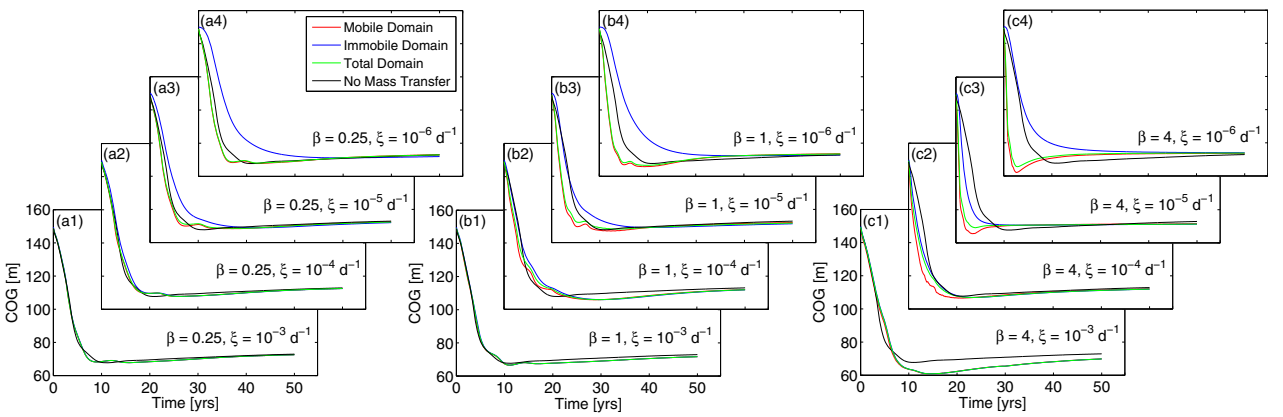

Figure 11. Sensitivity of β and ξ on the COG of the solute plume. (a1−a4) $\beta=0.25$; (b1−b4) $\beta=1$; and (c1−c4) $\beta=4$. For a specific β, $\xi=10^{-3}$, 10^{-4}, 10^{-5}, and $10^{-6}d^{-1}$.

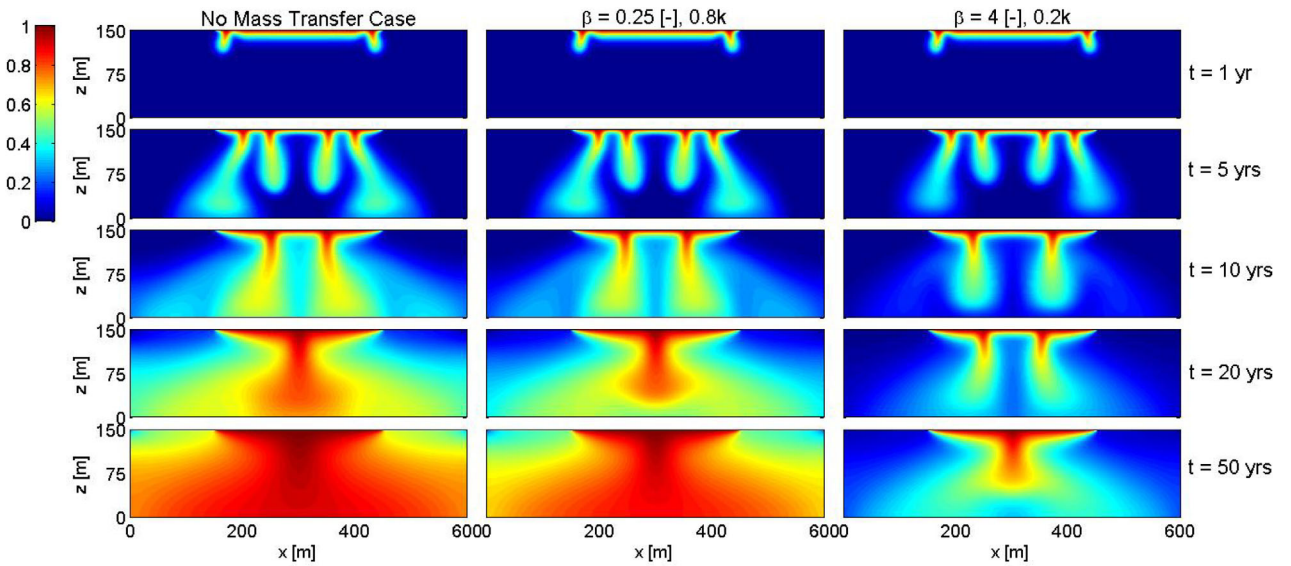

Figure 12. Concentration distributions of the cases with and without DDMT at simulation times of 1, 5, 10, 20, and 50 years. For the case including mass transfer, transient concentration distributions are shown in mobile domains. The capacity ratio and permeability of the mass transfer case in the middle column and the right column are: 0.25 and 0.8 k, and 4 and 0.2 k, respectively, in which k is the permeability of the no-mass-transfer case. For the two mass transfer cases, $\xi=10^{-5}d^{-1}$.

4.3. Consideration of the Permeability-Porosity Relationship

The results above are base on the assumption that permeability is independent of the mobile porosity. However, there is a close relationship between permeability and porosity (i.e., mobile porosity) in reality, which has been described by various empirical equations [e.g., *Costa*, 2006]. In general, permeability increases with increasing mobile porosity. For simplicity, we assume a simple linear relationship between the mobile porosity and permeability. This assumption leads to a constant *Ra* when varying the value of β. Figure 12 shows transient concentration distributions in the mobile domains in the no-mass transfer case and two mass transfer cases at simulation times of 1, 5, 10, 20, and 50 years. For the two mass transfer cases, $\beta=0.25$ and 4, implying that the values of porosity and permeability are 80% and 20% of those of the no-mass transfer case, respectively, with the consideration of the assumed relationship between permeability and porosity. In addition, $\xi=10^{-5}d^{-1}$ is adopted for both mass transfer cases.

As shown, the numbers of fingers at the simulation time of 1 year in these three cases are exactly the same, confirming that the value of *Ra* determines the instability of the system despite of different values in three cases. With increasing simulation time, however, the value of permeability dominates the plume evolution rate in the mobile domain. Specifically, a larger permeability corresponds to a higher rate of plume evolution in the mobile domain. Therefore, the largest rate occurs in the no-mass-transfer case and the least one in the mass transfer case with $\beta=4$. Due to the larger plume evolution rate in the mobile domain and a smaller immobile porosity, the plume in the immobile domain in the case with $\beta=0.25$ evolutes faster than in the case with $\beta=4$, as shown in Figure 13. As such, the transient *TM* is the largest in the no-mass-transfer case and the least in the case with $\beta=4$.

5. Summary and Conclusions

A numerical study has been conducted to investigate kinetic mass transfer effects on unstable density-driven flow and transport in porous media through a modified Elder problem. The first-order DDMT model coupled with the variable-density-flow model is employed to describe the transport behavior. Simulation results show that the effect of kinetic mass transfer on solute loading may be significant and varies highly depending on mass transfer parameters including capacity ratio and mass transfer rate coefficient. The main findings based on the assumption of a constant total porosity are as follows:

1. In comparison to the no-mass-transfer case, a higher degree of instability and a significantly more unstable system is developed in the mass transfer case, in which the total porosity remains the same as that in

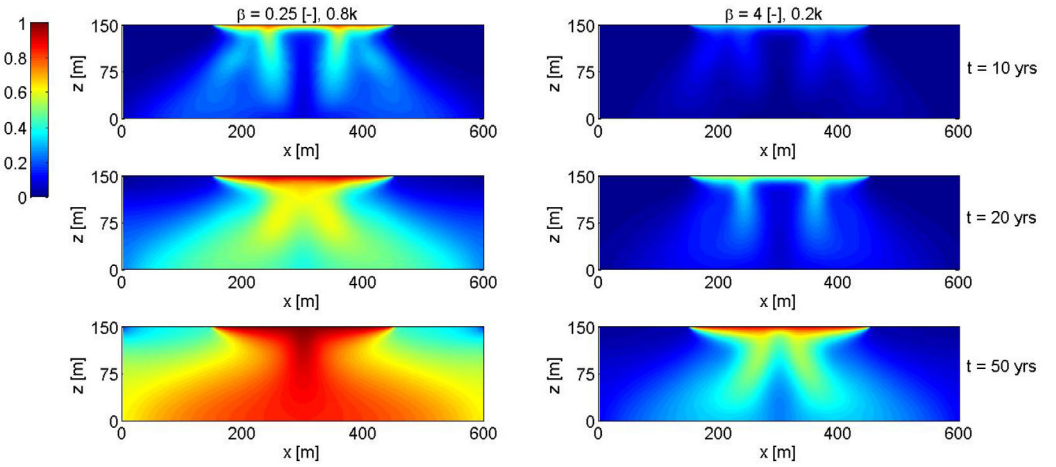

Figure 13. Transient concentration distributions in the immobile domains at simulation times of 10, 20, and 50 years. The capacity ratio and permeability of the mass transfer case in the left column and the right column are: 0.25 and 0.8 k, and 4 and 0.2 k, respectively, in which k is the permeability of the no-mass-transfer case. For the two mass transfer cases, $\xi=10^{-5}d^{-1}$.

the no-mass-transfer case. This is mainly caused by a reduced effective porosity and a corresponding larger Rayleigh number.

2. The magnitude of the capacity ratio (β) controls the macroscopic plume profile, while the magnitude of the mass transfer rate (ξ) determines the plume evolution rate. The higher the value of β, the more unstable the system. A larger ξ yields a lower mobile plume evolution rate. In addition, ξ dominates the average concentration difference between the mobile and immobile domains characterized by the nonequilibrium state index (*NESI*).
3. There are two mechanisms controlling solute transport: the density-driven transport in the mobile zone and local kinetic mass transfer between the mobile and immobile domains. The magnitude of β controls the mechanism driving solute loading. For a large β, solute loading is dominated by the density-driven transport, while with decreasing β local mass transfer dominated solute loading may occur at later times. At large times, however, these two mechanisms equally contribute to the solute loading.
4. In the presence of the immobile domain and associated kinetic mass transfer, the oscillations of the Sherwood Number (*Sh*) are enhanced and more significant in the case with a smaller β. The variation of average mobile concentration in the top boundary layer is an indicator of the variation of *Sh*, reflecting the stage of instability. *Sh* could be a nonmonotonic function of mass transfer timescale due to the complicated interactions between source zone, mobile zone and immobile zone in the top boundary layer. For a very large or very small ξ, mass transfer makes a very limited contribution to the enhancement of solute loading during the effective period (first 10 years in the current setting with $\beta=4$), while a critical ξ can cause the immobile concentration to increase from zero to mobile concentration during that period.
5. Without any exception, the inclusion of the immobile domain decreases the transient total mass (*TM*) in the aquifer system. For the case with a smaller β, the *TM* in the entire aquifer exhibits smaller variability for different ξ and is close to that in the no-mass-transfer case. With increasing β, by contrast, the *TM* in the entire aquifer is highly affected by the magnitude of ξ due to the increased contribution from the immobile zone. Also, the effect of ξ on the *TM* in the total and immobile domains may be nonmonotonic, which is similar to the effect on *Sh*.
6. In all cases, the solute centre of gravity (*COG*) initially decreases because of the descent of the first salt fingers, followed by a slight rebound after the first fingers touch the bottom of the aquifer, and finally asymptotically approaching the vertical centre (75m) of the domain. The *COG* in the total domain has a similar trend to that in the mobile domain, indicating that mobile concentration distribution determines the *COG* in the total domain.
7. When assuming that permeability increases linearly with the mobile porosity, *Ra* is constant regardless of the values of permeability and the mobile porosity, leading to the same instability of the unstable density-driven system. The rates of plume evolution in both mobile and immobile domains, however, are

higher in the aquifer system with higher permeability. Therefore, higher permeability results in a higher transient *TM*.

The DDMT model used in the current study is not new and has been extensively used in describing transport behavior in a wide variety of laboratory and field settings, this is the first application to an unstable variable-density flow problem. These initial results suggest that kinetic mass transfer is an important process and is expected to be important in other variable-density flow settings. Studies are required to explore the application of DDMT models to real-world unstable variable-density flow problems across a range of different hydrogeologic settings and spatial and temporal scales.

The DDMT model offers a physically based alternative to classic advection-dispersion models. However, the successful use of this model still remains a persistent challenge in all areas of solute transport modelling, particularly in the calibration of mass transfer parameters. Future work is also required to develop an effective method for estimating mass transfer parameters in variable-density flow problems. Moreover, as the DDMT model is capable of simulating the preferential movement of water and solutes in structured porous media, comparison of the application of the DDMT model and the discrete fracture network (DFN) in understanding, modelling and predicting free convection processes is of particular interest.

Acknowledgments
This work was supported by Open Research Fund Program of State Laboratory of Water Resources and Hydropower Engineering Science in China (2014NSG02) and the Fundamental Research Funds for the Central Universities (2015B28714). The data used in this paper can be obtained upon request from the corresponding author.

References

Ataie-Ashtiani, B., C. T. Simmons, and A. D. Werner (2014), Influence of boundary condition types on unstable density-dependent flow, *Ground Water*, *52*(3), 378–387, doi:10.1111/gwat.12067.
Berkowitz, B., and H. Scher (1997), Anomalous transport in random fracture networks, *Phys. Rev. Lett.*, *69*, 4038–4041.
Berkowitz, B., and H. Scher (1998), Theory of anomalous chemical transport in random facture networks, *Phys. Rev. E*, *57*, 5858–5869.
Blessent, D., P. R. Jørgensen, and R. Therrien (2014), Comparing discrete fracture and continuum models to predict contaminant transport in fractured porous media, *Ground Water*, *52*(1), 84–95.
Carrera, J., X. Sanchez-Vila, I. Benet, A. Medina, G. Galarza, and J. Guimera (1998), On matrix diffusion: Formulations, solution methods and qualitative effects, *Hydrogeol. J.*, *6*, 178–190.
Chambon, J. C. C., P. J. Binning, P. R. Jørgensen, and P. L. Bjerg (2011), A risk assessment tool for contaminated sites in low-permeability fractured media, *J. Contam. Hydrol.*, *124*(1–4), 82–98.
Chen, W. L., and R. J. Wagenet (1995), Solute transport in porous-media with sorption-site heterogeneity, *Environ. Sci. Technol.*, *29*, 2725–2734.
Coats, K. H., and B. D. Smith (1964), Dead-end pore volume and dispersion in porous media, *Soc. Pet. Eng. J.*, *4*, 73–81, doi:10.2118/647-PA.
Costa, A. (2006), Permeability-porosity relationship: A reexamination of the Kozeny-Carman equation based on a fractal pore-space geometry assumption, *Geophys. Res. Lett.*, *33*, L02318, doi:10.1029/2005GL025134.
Culkin, S. L., K. Singha, and F. D. Day-Lewis (2008), Implications of rate-limited mass transfer for aquifer storage and recovery, *Ground Water*, *46*, 591–605.
Dentz, M., and B. Berkowitz (2003), Transport behaviour of a passive solute in continuous time random walks and multirate mass transfer, *Water Resour. Res.*, *39*(5), 1111, doi:10.1029/2001WR001163.
Elder, J. W. (1967), Transient convection in a porous medium, *J. Fluid Mech.*, *27*(3), 609–623.
Feehley, C. E., C. Zheng, and F. Molz (2000), A dual-domain mass transfer approach for modelling solute transport in heterogeneous aquifers: Application to the Macrodispersion Experiment (MADE) site, *Water Resour. Res.*, *36*, 2501–2515.
Flach, G. P. (2011), Relationship between dual-domain parameters and practical characterization data, *Ground Water*, *50*(2), 216–229.
Frind, E. O. (1982), Simulation of long-term transient density-dependent transport in groundwater, *Adv. Water Resour.*, *5*, 73–88.
Gong, R., et al. (2010), Estimating kinetic mass transfer by resting-period measurements in flow-interruption tracer tests, *J. Contam. Hydrol.*, *117*, 37–45.
Graf, T., and R. Therrien (2005), Variable-density groundwater flow and solute transport in porous media containing nonuniform discrete fractures, *Adv. Water Resour.*, *28*, 1351–1367.
Haggerty, R., and S. M. Gorelick (1995), Multiple-rate mass-transfer for modelling diffusion and surface-reactions in media with pore-scale heterogeneity, *Water Resour. Res.*, *31*, 2383–2400.
Haggerty, R., S. A. Mckenna, and L. C. Meigs (2000), On the late-time behaviour of tracer test breakthrough curves, *Water Resour. Res.*, *36*, 3467–3479.
Harvey, C. F., and S. M. Gorelick (2000), Rate-limited mass transfer for macrodispersion: Which dominates plume evolution at the Macrodispersion Experiment (MADE) site?, *Water Resour. Res.*, *36*, 637–650.
Holzbecher, E. (2005), Groundwater flow pattern in the vicinity of a salt lake, *Hydrobiologia*, *532*, 233–242.
Horton, C. W., and F. T. Rogers (1945), Convection currents in a porous medium, *J. Appl. Phys.*, *16*, 367–370.
Koch, M., and G. Zhang (1992), Numerical solution of the effects of variable density in a contaminant plume, *Groundwater*, *30*, 731–742.
Kooi, H., J. Groen, and A. Leijnse (2000), Modes of seawater intrusion during transgressions, *Water Resour. Res.*, *36*, 3581–3589.
Langevin, C. D., W. B. Shoemaker, and W. Guo (2003), Modflow-2000, The U.S. Geological Survey modular ground-water flow model–Documentation of the Seawat-2000 version with the variable density flow process (VDF) and the integrated MT3DMS transport process (IMT), *U.S. Geol. Surv. Open File Rep.*, *03-426*, 43 pp.
Lapwood, E. R. (1948), Convection of a fluid in porous medium, *Proc. Cambridge Philos. Soc.*, *44*, 508–521.
Liu, G., C. Zheng, and M. Gorelick (2007), Evaluation of the applicability of the dual-domain mass transfer model in porous media containing connected high-conductivity channels, *Water Resour. Res.*, *43*, W12407, doi:10.1029/2007WR005965.
Liu, H. H., and J. H. Dane (1996), A criterion for gravitational instability in miscible dense plumes, *J. Contam. Hydrol.*, *23*, 233–243.
Liu, Y., X. Kuang, J. J. Jiao, and J. Li (2015), Numerical study of variable-density flow and transport in unsaturated-saturated porous media, *J. Contam. Hydrol.*, *182*, 117–130.

Lu, C., and J. Luo (2010), Dynamics of freshwater-seawater mixing zone development in dual-domain formations, *Water Resour. Res.*, *46*, W11601, doi:10.1029/2010WR009344.
Lu, C., P. K. Kitanidis, and J. Luo (2009), Effects of kinetic mass transfer and transient flow conditions on widening mixing zones in coastal aquifers, *Water Resour. Res.*, *45*, W12402, doi:10.1029/2008WR007643.
Lu, C., P. Du, Y. Chen, and J. Luo (2011), Recovery efficiency of aquifer storage and recovery (ASR) with mass transfer limitation, *Water Resour. Res.*, *47*, W08529, doi:10.1029/2011WR010605.
Neville, C. J. (2006), *Modeling Dual-Domain Transport With MT3D*, S.S. Papadpulos & Associates, Inc.
Nield, D. A., and A. Bejan (2006), *Convection in Porous Media*, 4th ed., Springer, Berlin.
Nield, D. A., and C. T. Simmons (2007), A discussion on the effect of heterogeneity on the onset of convection in a porous medium, *Transp. Porous Media*, *68*, 413–421.
Park, C. H., and M. M. Aral (2003), Sensitivity of the solution of the Elder problem to density, velocity and numerical perturbations, *J. Contam. Hydrol.*, *92*, 33–49.
Post, V. E. A., and H. Prommer (2007), Multicomponent reactive transport simulation of the Elder problem: Effects of chemical reactions on salt plume development, *Water Resour. Res.*, *43*, W10404, doi:10.1029/2006WR005630.
Post, V. E. A., and C. T. Simmons (2010), Free convection controls on sequestration of salts into low-permeability strata: Insights from sand tank laboratory experiments and numerical modelling, *Hydrogeol. J.*, *18*, 39–54.
Prasad, A., and C. T. Simmons (2003), Unstable density-driven flow in heterogeneous porous media: A stochastic study of the Elder [1967b] ''Short heater'' problem, *Water Resour. Res.*, *39*(1), 1007, doi:10.1029/2002WR001290.
Prasad, A., and C. T. Simmons (2005), Using quantitative indicators to evaluate results from variable-density groundwater flow models, *Hydrogeol. J.*, *13*, 905–914.
Salamon, P., D. Fernandez-Garcia, and J. J. Gomez-Hernandez (2006),. Modeling mass transfer processes using random walk particle tracking, *Water Resour. Res.*, *42*, W11417, doi:10.1029/2006WR004927.
Schincariol, R. A. (1998), Dispersive mixing dynamics of dense miscible plumes: Natural perturbation initiation by local-scale heterogeneities, *J. Contam. Hydrol.*, *34*, 247–271.
Schincariol, R. A., and F. W. Schwartz (1990), An experimental investigation of variable density flow and mixing in homogeneous and heterogeneous media, *Water Resour. Res.*, *26*, 2317–2329.
Schincariol, R. A., F. W. Schwartz, and C. A. Mendoza (1997), Instabilities in variable density flows: Stability analyses for homogeneous and heterogeneous media, *Water Resour. Res.*, *33*, 31–41.
Sharp, J. M., and M. Shi (2009), Heterogeneity effects on possible salinity-driven free convection in low-permeability strata, *Geofluids*, *9*, 263–274, doi:10.1111/j.1468-8123.2009.00262.x.
Shikaze, S. G., E. A. Sudicky, and F. W. Schwartz (1998), Density-dependent solute transport in discretely-fractured geological media: Is prediction possible?, *J. Contam. Hydrol.*, *34*, 273–291.
Simmons, C. T. (2005), Variable density groundwater flow: From current challenges to future possibilities, *Hydrogeol. J.*, *13*(1), 116–119.
Simmons, C. T., and K. A. Narayan (1997), Mixed convection processes below a saline disposal basin, *J. Hydrol.*, *194*, 263–285.
Simmons, C. T., T. R. Fenstemaker, and J. M. Sharp Jr. (2001), Variable density groundwater flow and solute transport in heterogeneous porous media: Approaches, resolutions and future challenges, *J. Contam. Hydrol.*, *52*, 245–275.
Simmons, C. T., J. M. Sharp, and D. A. Nield (2008), Modes of free convection in fractured low-permeability media, *Water Resour. Res.*, *44*, W03431, doi:10.1029/2007WR006551.
Stevens, J. D., J. M. Sharp, C. T. Simmons, and T. R. Fenstemaker (2009), Evidence of free convection in groundwater: Field-based measurements beneath wind-tidal flats, *J. Hydrol.*, *375*, 394–409.
Thorne, D. T., and A. C. Sukop (2004), Lattice Boltzmann model for the Elder problem, paper presented at 15th International Conference on Computational Methods in Water Resources, Chapel Hill, N. C., 13–17 Jun., *Developments in Water Science, 55*(2), 1549–1557, doi: 10.1016/S0167-5648(04)80165-5.
Van Dam, R. L., C. T. Simmons, D. W. Hyndman, and W. W. Wood (2009), Natural free convection in porous media: First field documentation in groundwater, *Geophys. Res. Lett.*, *36*, L11403, doi:10.1029/2008GL036906.
van Genuchten, M. T., and P. J. Wierenga (1976), Mass-transfer studies in sorbing porous-media: 1. Analytical solution, *Soil Sci. Soc. Am. J.*, *40*, 473–480.
van Reeuwijk, M., S. A. Mathias, C. T. Simmons, and J. D. Ward (2009), Insights from a pseudospectral approach to the Elder problem, *Water Resour. Res.*, *45*, W04416, doi:10.1029/2008WR007421.
Voss, C. I., and W. R. Souza (1987), Variable density flow and solute transport simulation of regional aquifers containing a narrow freshwater-seawater mixing zone, *Water Resour. Res.*, *23*, 1851–1866.
Vujevic, K., T. Graf, C. T. Simmons, and A. D. Werner (2014), Impact of fracture network geometry on free convection flow patterns, *Adv. Water Resour.*, *71*, 65–80.
Wood, J. R., and T. A. Hewett (1984), Reservoir diagenesis and convective fluid flow, in *Clastic Diagenesis, AAPG Mem. 37*, edited by D. A. McDonald and R. C. Surdam, pp. 99–111, Amer. Assoc. Petrol. Geol., Tulsa, Okla.
Wooding, R. A., S. W. Tyler, and I. White (1997), Convection in groundwater below an evaporating salt lake: 1. Onset of instability, *Water Resour. Res.*, *33*, 1199–1217.
Xie, Y., C. T. Simmons, A. D. Werner, and J. Ward (2010), Effects of transient solute loading on free convection in porous media, *Water Resour. Res.*, *46*, W11511, doi:10.1029/2010WR009314.
Xie, Y., C. T. Simmons, and A. D. Werner (2011), Speed of free convective fingering in porous media, *Water Resour. Res.*, *47*, W11501, doi: 10.1029/2011WR010555.
Xie, Y., C. T. Simmons, A. D. Werner, and H.-J. G. Diersch (2012), Prediction and uncertainty of free convection phenomena in porous media, *Water Resour. Res.*, *48*, W02535, doi:10.1029/2011WR011346.
Yang, J., and R. N. Edwards (2000), Predicted groundwater circulation in fractured and unfractured anisotropic porous media driven by nuclear fuel waste heat generation, *Can. J. Earth Sci.*, *37*, 1301–1308.
Zhang, H. B., and F. W. Schwartz (1995), Multispecies contaminant plumes in variable-density flow systems, *Water Resour. Res.*, *31*, 837–847.
Zinn, B., L. C. Meigs, C. F. Harvey, R. Haggerty, W. J. Peplinski, and C. F. Von Schwerin (2004), Experimental visualization of solute transport and mass transfer processes in two-dimensional conductivity fields with connected regions of high conductivity, *Environ. Sci. Technol.*, *38*, 14, 3916–3926.